Determination of *in situ* trap properties in CCDs using a "single-trap pumping" technique

Determination of in situ trap properties in CCDs using a "single-trap pumping" technique

David J. Hall, Neil J. Murray, Andrew D. Holland, Jason Gow, Andrew Clarke and David Burt

***Abstract*—The science goals of space missions from the Hubble Space Telescope through to Gaia and Euclid require ultra-precise positional, photometric and shape measurement information. However, in the radiation environment of the space telescopes, damage to the focal plane detectors through high energy protons leads to the creation of traps, a loss of charge transfer efficiency and a consequent deterioration in measurement accuracy. An understanding of the traps produced and their properties *in* the CCD during operation is essential to allow optimisation of the devices and suitable modelling to correct the effect of the damage through the post-processing of images. The technique of "pumping single traps" has allowed the study of *individual* traps in high detail that cannot be achieved with other techniques, such as Deep Level Transient Spectroscopy, whilst also locating each trap to the sub-pixel level in the device. Outlining the principles used, we have demonstrated the technique for the A-centre, the most influential trap in serial read-out, giving results consistent with the more general theoretical values, but here showing new results indicating the spread in the emission times achieved and the variation in capture probability of individual traps with increasing signal levels. This technique can now be applied to other time and temperature regimes in the CCD to characterise individual traps in situ under standard operating conditions such that dramatic improvements can be made to optimisation processes and modelling techniques.**

***Index Terms*—A-centre, CCD image sensors, defect, pocket pumping, radiation damage, Si-A, Euclid, trap pumping**

I. Introduction

With the science goals of space missions such as Euclid [1] and Gaia [2] becoming ever more demanding, the precision required from the instruments on board becomes ever greater. The imaging sensor of choice for many missions is the Charge-Coupled Device (CCD). However, CCDs suffer from radiation damage when in orbit due to the space radiation environment. The radiation induces traps in the silicon that can capture electrons from the signal charge packets and subsequently release the captured electrons at a later time (determined by the emission time-constant for said trap). This capture and release leads to a deterioration of the charge transfer efficiency resulting in the smearing of the images, such as that shown in Figure 1 (left) [3]. As the traps appear to be fundamental to the silicon and inherent in the CCDs when irradiated, two methods are currently being used to reduce the impact on the science goals: optimisation of the operating conditions (such as changing the clocking schemes to reduce the impact of charge deferral as shown in [4]) and simulation of the damage such that the damaged image can be iterated back to the effectively undamaged image as detailed in [5], [6] and [7]. In both cases moving forwards, a thorough understanding of the trap properties in the CCD is essential.

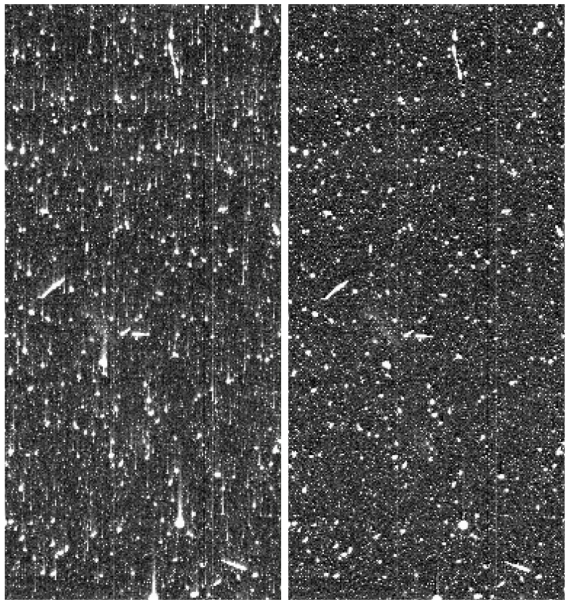

Fig. 1. A typical raw ACS/WFC science exposure from early 2010 (HST-GO-11689, PI: Renato Dupke) before (left) and after (right) CTI correction. The 380×820 pixel area selected is furthest on the detector from the readout register, and the logarithmic colour scale is chosen intentionally to highlight the CTI trails. Figure and caption reproduced from R. Massey. *MNRAS* (2010) Vol. 409 L109-L113, Fig. 3 [3]. By permission of Oxford University Press on behalf of the Royal Astronomical Society.

The Hubble Space Telescope (HST) uses forward modelling of the radiation-induced smearing process to correct the images, as detailed in Table 1 of [5]. The aim of the scheme is to return electrons to the pixels from which they were "unintentionally dragged during readout" in raw images; the science results are not corrected directly, but are corrected through the modification of the raw data. For HST, these methods can reduce charge trails by approximately 30 times, Figure 1 (right) [3], using appropriate trap parameters.

Gaia will chart a three-dimensional map of our Galaxy with the aim of revealing its composition, formation and evolution [2]. The consequences of poor transfer efficiency are that centroids are deferred in time and therefore give rise to positional changes. Without correction, the science goals could not be achieved and therefore one of the major challenges to

D. J. Hall, N. J. Murray, A. Holland, J. Gow and A. Clarke are with the *e2v centre for electronic imaging*, Department of Physical Sciences, The Open University, Milton Keynes, UK (email: david.hall@open.ac.uk; n.j.murray@open.ac.uk; andrew.holland@open.ac.uk; jason.gow@open.ac.uk; andrew.clarke@open.ac.uk).

D. Burt is with *e2v technologies*, 106 Waterhouse Lane, Chelmsford, Essex, CM1 2QU (email: david.burt@e2v.com).

the mission will be the correction of the radiation induced damage. With high volumes of data requiring correction, a model is used that describes the effects of the radiation damage in a physically realistic manner whilst allowing fast enough processing. To this end, the Charge Distortion Model (CDM) was developed for the mission [7]. By considering the signal history and applying Shockley-Read-Hall theory (Section II) using a "column-averaged" approach, it does not consider individual traps independently but many traps as having an impact along the length of the column as one.

Euclid aims to map the geometry of the dark universe to help answer the question of how the universe originated, as detailed in [1] and [8]. One method used to investigate this geometry is through the measurement of subtle changes in ellipticity caused by weak gravitational lensing. The Euclid focal plane will suffer from radiation damage in much the same way as Gaia and HST [9], distorting the measurements beyond the required sensitivity. Although a 90% correction of the charge trailing was achieved for HST Advanced Camera for Surveys data from 2006, and more recently an updated model achieved a 97% correction in data from 2010 [5], Euclid will require 99% correction (see [1], [10] and [11]). The correction achievable depends on the accuracy of the CCD CTI model [11], and therefore requires more accurate trap parameters that those required for HST.

As the science goals for missions become increasingly dependent on correction against radiation damage, a greater accuracy in trap parameters is required. To determine these trap parameters to the accuracy needed moving forwards, new methods are required to provide details of *individual* traps and not average-properties [12].

II. Radiation Damage

In orbit, the CCD is continuously bombarded by high energy protons. These protons can cause displacement damage in the silicon and cause the development of traps, as detailed in [13]. The traps that are produced in the buried channel of the CCD can capture electrons from the signal charge as it passes through the device. Such captured charge can then be released at a later point in time, causing the smearing seen in images from HST before correction, as shown in Figure 1 [3].

The capture and emission of electrons can be described by Shockley-Read-Hall (SRH) theory, see [14] and [15], and modelled through the use of two exponential time constants: the capture time constant τ_c (Equation 1) and emission time constant τ_e (Equation 2), where m_{dos} and m_c are the density of states and conductivity effective masses of the electron respectively, v_{th} is the thermal velocity, σ is the capture cross-section, n is the electron concentration, where x can be replaced with c or e for capture and emission respectively. X is the entropy factor that is associated with the entropy change for electron emission from the trap and χ is a factor added to allow for any field enhanced emission which can affect the trap emission time as well as dark current generation [16]. These expressions can be used to calculate the probability of capture and emission of charge in a given time t (Equation 5). The emission time τ_e of the traps determines the probability that captured charge will be emitted into a subsequent charge packet and not return to that from which it was captured (resulting in no net change to the signal).

$$\tau_c = \frac{1}{\sigma n v_{th}} \tag{1}$$

$$\tau_e = \frac{1}{X\chi\sigma N_c v_{th}} \exp\left(\frac{E}{kT}\right) \tag{2}$$

$$N_c = 2\left(\frac{2\pi m_{dos} kT}{h^2}\right)^{\frac{3}{2}} \tag{3}$$

$$v_{th} = \sqrt{\frac{3kT}{m_c}} \tag{4}$$

$$P_x = 1 - exp\left(\frac{-t}{\tau_x}\right) \tag{5}$$

The energy levels below the conduction band of known traps in n-channel CCDs of significance to common readout and integration time-scales range from approximately 0.17-0.46 eV (from the Si-A to the Si-E respectively) [17]. It is very important to note the accuracy required in the energy levels of traps and how this impacts the emission time constants of the traps. An error in the energy level of the trap of only 0.01 eV at 153 Kelvin results in a factor of two variation in the emission time constant inferred. The emission times of traps required for accurate correction of radiation damage induced effects is of a high priority for CTI correction models, hence the accurate determination of these parameters is essential to many missions. In this study, we concentrate on determining the emission time constants, found in the time-domain directly. It is the emission time constants that are of greatest importance due to their direct use as a parameter in the HST [5] and Gaia [7] CTI mitigation procedures and not the energy levels.

III. Pocket pumping

The pocket pumping technique can be used to characterise different charge trap types and is often used to study potential pockets in a device [18]. Pocket pumping involves exposing the CCD to a flat field of signal (100-1000 electrons is suggested in [18]) and clocking the CCD backwards a specified number of lines before returning to the original position; this clocking is then repeated for many cycles. During the clocking cycle, charge builds up (or "pumps") at a trapping site with the rate of build-up directly proportional to the trap size. A similar process can also be used on individual radiation-induced traps. As the process is used in this study to examine individual traps it will henceforth be referred to as "trap pumping".

IV. Trap pumping

As a charge packet first passes over the trap it may capture an electron. This electron capture causes the signal packet from which it was captured to have one electron less. If the electron is emitted at a time when the closest charge packet is that from which it was captured then there will be no net change in the signal level in any of the charge packets. However, if the electron is emitted when the charge packet from which it

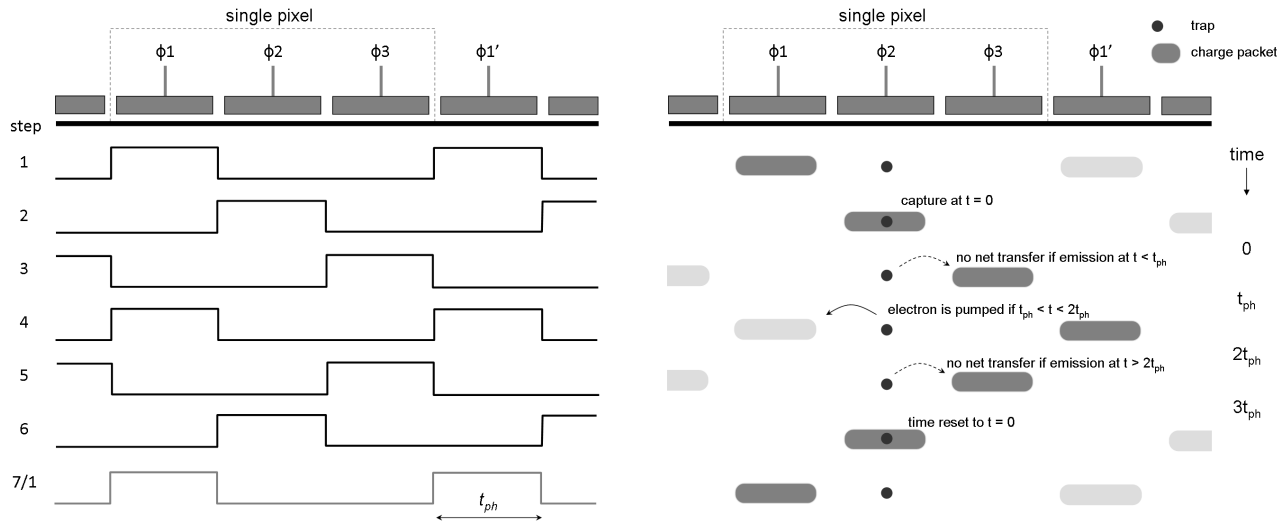

(a) Trap pumping clocking scheme.

(b) Trap pumping dynamics.

Fig. 2. Pumping from phases 1, 2, 3, 1', 3, 2 and back to 1 produces signal dipoles with the polarity of the dipole dependent on the trap location (under phase 2 or phase 3), where 1' denotes the first phase in the next pixel. An example of such dipoles achieved with the presented clocking scheme (mean signal level subtracted) is shown in Figure 3(a). (a) Steps 1-7 denote one cycle, with step 7 starting the next cycle. (b) The time is set to zero at the point at which the signal charge packet moves away from the trap (i.e. if the trap emits whilst in contact with the charge packet the trap is considered to instantly recapture). Using the clocking scheme shown in (a), pumping of an electron from one charge packet to the next will only occur between times $t = t_{ph}$ and $t = 2t_{ph}$.

was captured is *not* the closest then the electron will join a different charge packet. The charge packet that is joined will increase in signal by one electron, with the charge packet from which it was captured remaining without this electron.

The trap pumping mechanism enables the study of individual traps in the silicon, detailing their position to the electrode level in the device. This process allows device-level optimisation to be investigated such as clock timing adjustment to reduce deferred charge during read out [19]. This has major advantages over other techniques used to determine averaged trap properties on a larger scale, such as Deep Level Transient Spectroscopy (DLTS) [20] for which the trap properties may not be the same as those in the CCD (e.g. differences in the electric field or different doping in the device causing different trap concentrations). Using trap pumping, one can study the traps in close-to operation conditions for which the traps detected are therefore the traps most likely to affect star or galaxy images in a space mission. In principle, one could perform the trap pumping measurement in space during mission operation if the electronics and irradiation dose received allow, as suggested in [19] .

For demonstration purposes, consider the transfer of charge packets in a three-phase CCD through phases 1, 2, 3, 1', 3, 2 and back to 1 (one pumping cycle), where 1' denotes the first phase in the next pixel, Figure 2(a). This cycle can be repeated many times; for this example we will consider repeating this transfer 10 000 times. Clocking the device in this way gives rise to a high-low signal dipole in the image at the location of each trap, Figure 3(a). Only traps that are under phases 2 and 3 will show as intense dipoles in this case, with the polarity of the dipole (high-low or low-high) dependent on which phase the trap is under (phase 2 and phase 3 respectively).

Previous studies using pocket/trap pumping have demonstrated some of the strengths of the technique. In early studies, charge has been shifted over several pixels, creating bright pixels neighbouring several darker pixels from which charge was lost [21]. Using this form of the technique, one can measure a histogram of the bright and dark pixels at varying temperatures. An investigation of the so-called 'trap effectiveness' (pumped signal level) with varying temperature gives an indication of the trap species present and a time constant can be inferred using calculations with other parameters. More recently, charge has been transferred from one pixel to the next, as above, using transfer times of approximately 1 ms and 1 µs to represent the parallel and serial directions respectively [22]. Using a similar 'trap efficiency', measured as the average peak signal following pumping, one can trace the efficiency across a range of temperatures. On a pixel-by-pixel basis the trap efficiency can be tracked as a function of temperature, allowing a fitting of the trap energy and cross-section and consequently a calculation of the time constant. The process of creating high-low signal dipoles can also be used to determine the location and density of traps. In these cases, the density of the electron charge cloud is assumed constant and assumed to provide sufficient probability of instantaneous trapping.

In this study, we operate the trap pumping process in such a way that, with a comparison to an analytical methodology, one can determine the trap emission time constants to a high accuracy whilst also allowing the study of further properties of the trap that are essential to the success of future missions, such as the capture efficiency dynamics. Here, we trace the pumped signal as a function of the clock-width at each temperature (using even clock widths), Figure 2(a), thus studying the trap emission *in the time-domain*; the emission time constant, as one of the most important parameters, is now being considered without further knowledge of other properties

of the trap required and thus removing the propagation of any associated errors in the trap parameters used. By taking the process further and analysing the pumping-dynamics as a function of the signal density it is possible to determine the capture probability of individual traps with increasing signal levels and therefore gain further insight into each individual trap in the silicon. In the serial register with pixel transfer times of the order of 1 µs, it is not the case that instantaneous trapping can be considered, as seen later in this paper.

V. Analytical approach

One can consider the example given above from an analytical viewpoint. Consider a trap under phase 2 in the CCD, with the CCD clocked as suggested above with even clock timings such that the charge sits under each phase for a time t_{ph} before moving to the next phase, Figure 2(a). As the signal charge packet transfers from phase 1 to phase 2 this trap will capture an electron subject to sufficient electron density in the location where the trap is present; in this case we shall initially consider that there is 100% probability of capture, with consideration of the more general case following. In each cycle, charge is only pumped from one image pixel to the next if the trap emits within a time period of between $t = t_{ph}$ and $t = 2t_{ph}$ after leaving the first phase (defined as $t = 0$), Figure 2(b). The time is reset to $t = 0$ when the charge packet passes over the trap again such that if the trap emits it is considered to instantly recapture. As the trap is considered to have 100% probability of capture, the probability of the trap being filled at the point in time when the charge moves away from the trap is also 100%; the time can therefore be considered to be $t = 0$ at this point (i.e. when the charge moves from phase 2 to phase 3 in the example shown in Figure 2(b)). Calculating the probability of emission over time period for which the electron would be "pumped" and would not return to the original charge packet for a trap with emission time τ_e using Equation 5, one arrives at a probability of pumping which we will call P_p, Equation 6.

$$P_p = exp\left(\frac{-t_{ph}}{\tau_e}\right) - exp\left(\frac{-2t_{ph}}{\tau_e}\right) \tag{6}$$

Following a number of pumping cycles N, the amplitude I of the dipole will be given simply by $I = NP_p$ if there is a 100% probability of capture. To a first approximation, if the trap does not capture with 100% probability but instead captures with a probability P_c for a set signal level then this can be incorporated as a simple linear scaling factor, giving Equation 7.

$$I = NP_c\left(exp\left(\frac{-t_{ph}}{\tau_e}\right) - exp\left(\frac{-2t_{ph}}{\tau_e}\right)\right) \tag{7}$$

If I is tracked over a range of clocking widths t_{ph} then one can probe the emission time parameter space. Considering a range of clocking widths t_{ph} such as to surround the expected trap emission time, one is able to produce a curve such as that shown in Figure 3(b). A Monte Carlo simulation of the trap pumping process has been produced, taking into account electron transfer, capture and release, based on [23]. The results match the analytical solution directly (Figure 3(b)) and the Monte Carlo simulation can then be used to consider more complex solutions in which several traps are present under the same phase or in neighbouring phases. By differentiating Equation 7, one can see that the peak of the pumped signal amplitude lies at $\tau_e \ln 2$, in agreement with the Monte Carlo model, Figure 3(b). However, in the case presented here, where we are examining individual traps separated by several phases, a more efficient solution to obtaining parameters is to use a least-squares fitting method of the analytical solution to the curve, with particular reference to the noise in the data and the finite resolution of t_{ph} achievable (limited here by the drive electronics at the shorter end of the time-scales tested).

VI. Probing the charge packet geometry

A major benefit of this method is that one can probe individual traps located within the CCD. Not only can the location and emission properties of the trap be probed however, as one can also consider the capture properties of the trap; if the signal level is varied then the probability of capture can be probed. If a trap is located within the centre of the charge storage location then the probability of capture can be considered to be 100 % with each transfer at transfer times of approximately 1 µs, assuming of course that the trap is empty. For traps away from the centre of the signal packet as it moves through the device, the dynamics are more complicated and the capture probability may not be 100%, particularly with faster transfer times, contrary to the assumptions of the previous studies mentioned in Section IV. The density of the charge packet decreases as you move away from its centre and therefore this has a direct impact on the capture probability as defined in Equation 1. As the number of electrons in the charge packet increases, the volume encompassed by the electrons and the electron density at each point increases, as discussed in [24] and [25]. Therefore, as the size of the charge packet increases, one would expect the capture probability to increase for the same trap location up to a peak value of 100% within the time scales and signal levels of interest.

Although the capture probability can be measured directly (i.e. from the fitting of the analytical function), it should be noted that this includes a contribution from the electron density at the trap location *and* the capture cross-section of the trap; a trap at the centre of the pixel with a small cross-section might behave similarly to a trap near the edge of the pixel with a larger cross-section (under a specific set of operating conditions). However, if one considers that the traps are uniformly distributed throughout the buried channel and that for a given emission time constant or narrow range of time constants we are looking at one trap species (as a different trap species with different energy level or capture cross-section would behave differently with varying temperature), it is possible to investigate the charge packet-geometry. By considering the distribution of the capture probability against increasing signal levels across many traps and combining this with a uniform distribution of traps, one can measure the variation in capture probability with increasing signal size and provide further experimental calibration of the signal-volume models discussed above. In order to determine the capture

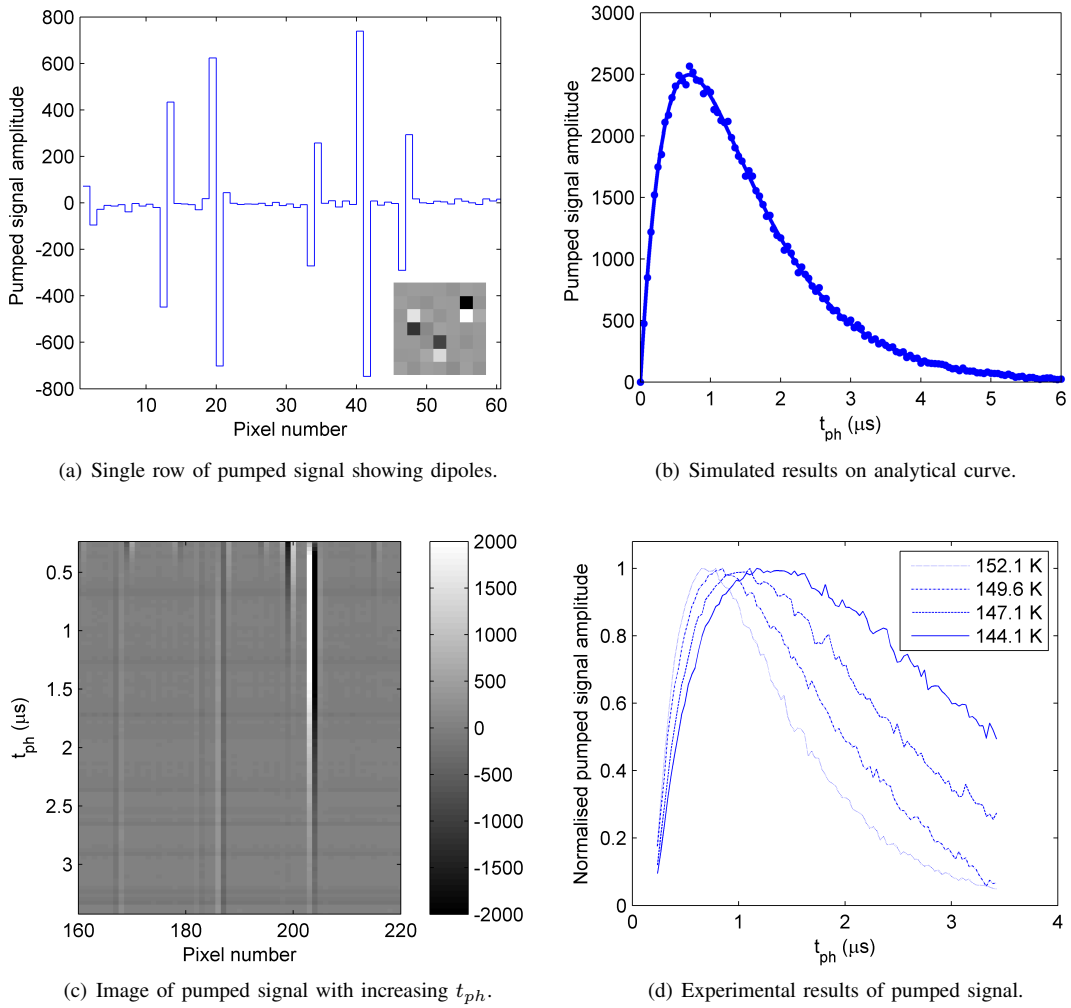

(a) Single row of pumped signal showing dipoles.

(b) Simulated results on analytical curve.

(c) Image of pumped signal with increasing t_{ph}.

(d) Experimental results of pumped signal.

Fig. 3. (a) An example line-plot of pumped dipoles (mean signal level subtracted) demonstrating three low-high and two high-low dipoles and, inset, how three traps might look in an image. (b) Pumping over a range of clock timing widths t_{ph} in Equation 7 produces a curve as shown by the solid line, here for the case of 10 000 pump cycles with an emission time constant of $\tau_e = 1$ µs. A Monte Carlo simulation of the same pumping conditions was produced based on [23], giving the data points on the plot. (c) A section of the image stacks produced from the experimental data. The variation in amplitude of the black-white stripe pairs with increasing t_{ph} relate to the same profiles as that shown simulated in Figure 3(b). The trap shown at pixel number 203 gives a clear amplitude profile that is shown in Figure 3(d) across four different temperatures. (d) The amplitude profile for the trap located at pixel 203, Figure 3(c), across four temperatures. As the temperature increases the peak in the profile (proportional to the trap emission time) decreases as expected from SRH theory.

cross-section of said traps one must then consider a fit to the emission time variation with temperature in a similar way to that used in the previous studies detailed in Section IV.

VII. Experimental results

In order to verify the analytical solution and Monte Carlo simulation, a series of experimental tests were implemented. Consider the A-centre in silicon, with a trap energy level below the conduction band of 0.17 eV [17]. This energy, under no electric field, gives an emission time of approximately 0.2 µs at 153 Kelvin, a timing which is of the same order as the standard serial register clock timings in the CCD and therefore of vital importance to CCD readout optimisation.

Considering the A-centre (Si-A) due to the dominance of this trap in the serial register in standard CCD readout timings (of the order of microseconds), a test matrix of pumped images was produced over a range of 20 signal amplitudes, from approximately 1k electrons to 20k electrons per pixel, across a range of 100 phase times (from approximately 200 ns to 3.4 µs in 32 ns steps). Four temperatures were employed (152.1, 149.6, 147.1 and 144.1 $\pm$ 0.2 Kelvin) to ensure that the traps behaved as expected theoretically across varying temperatures.

Pumping the three-phase serial register of the control region of a proton-irradiated CCD273 [26] (i.e. behind shielding during irradiation and therefore non-irradiated), stacked "images" were produced; a small area sample is shown in Figure 3(c). Several black-white stripe pairs can be seen, each due to a trap under a phase in the CCD; each row in the image shown in Figure 3(c) is equivalent to the line plot shown in Figure 3(a). Although the non-irradiated region of the device was used in this study, the process can be repeated on irradiated regions of a device, albeit regions that have been subjected to a low radiation dose; the dose to which this device was irradiated (of the order of 10^{10} protons cm^{-2} 10 MeV equivalent, done so for a separate study) was found to be too high for use of the technique in the irradiated region in this case. However,

one can see in Figure 3(c) that there is a lot of space in the non-irradiated region between traps containing pixels in which additional radiation-induced traps could be analysed. Moving down the plot from the top to bottom, each row represents a new clock width timing t_{ph}. The more efficient the pumping at each timing, the darker/brighter the black/white strip will be and the higher the amplitude of the pumped signal. Taking the trap demonstrated by the white stripe at pixel number 203 as an example, a similar amplitude profile can be tracked through t_{ph} as that shown in Figure 3(b). The strong response of the trap at pixel 203 from Figure 3(c) can be profiled through the bright-side of the dipole and plotted at each temperature, Figure 3(d). As the temperature increases, the peak in the profile shifts to lower time-scales, giving shorter emission time constants as one would expect.

Several dipoles can be seen only at t_{ph} values below 0.5 µs; these traps have very short emission time constants and therefore are not important for standard CCD readout rates. Charge captured by traps with very short emission time constants relative to t_{ph} will immediately be released back into the charge packet as it moves away from the trap location.

Taking the approximately 50 traps sampled in the experimental data, the emission time constants can be found for each individual trap and tracked across the temperature range in question using a least-squares fit to the analytical solution presented in Equation 7. With the traps sampled across increasing signal amplitudes, information can be retrieved regarding the position of the trap under the phase in relation to the trap capture probability and therefore how central the trap is to the signal charge packet position under each phase.

It should be noted that charge packets being stored and transferred in a CCD do not have well-defined edges; there is no strictly definable volume to the charge packet. As seen in Figure 4(b), the charge packet has so-called "fuzzy edges". This variation in electron density across the charge packet gives rise to a variation in the capture time constant, and therefore the capture probability, from one point in space to another. By probing the capture probability using the trap pumping methodology detailed above, one can begin to gain an insight into where the trap is located in relation to the charge packet under each electrode. Furthermore, it is possible, through the pumping of traps across different signal levels, to vary the electron density at each trap location. The probing of the traps at this level gives a new and vital experimental insight into the way by which the charge packet geometry varies with an increasing number of electrons, providing a useful addition to previous studies in this area such as [23], [24] and [25]. The variation in trapping "efficiency" shown in Figure 5(b) shows the variation in trapping probability with increasing signal level. This measure of capture probability with increasing signal level is an essential input to charge transfer models, particularly to meet the strict signal-volume parameter requires for future missions as discussed previously.

Results for several of the traps sampled in the serial register are shown in Figure 5. Collating the results for all sampled traps provides an insight into the variation in the trap emission times, here for what are expected to be the Si-A traps in the serial register of the CCD, Figure 6(a). A small number of traps appear to show no τ_e variation with temperature and it is thought that these results may occur due to other factors, for example, traps in two adjacent phases pumping against each other. Figure 6(b) shows a histogram of the measured time constants that were demonstrated in Figure 6(a).

The spread of the calculated emission time constants is thought to be real and not a consequence of, for example, poor fitting. There are no systematic shifts from one pixel to the next inside the same CCD; the different values of the emission time constant from one trap to the next follow no trend across the device (i.e. there is no influence from, for example, non-uniform cooling across the device). Each trap follows the expected trend with temperature with a very low variation from one temperature measurement to the next despite each temperature measurement being made during a different week of testing. As the trend remains with very small deviations from the form of the curves predicted by Equation 2, the errors in the values calculated have been estimated (as deviations from fitted curves with temperature dependence as in Equation 2) of between 4-6% (this value includes the contribution from all other sources of error such as fitting accuracy of the analytical equation to measure the emission time constants). Alongside increasing the number of repeats of the measurements in the device, it is expected that these errors can be reduced much further through reducing the main source of error in the measurements made: the sampling of t_{ph}, particularly at the faster end of the spectrum. With the system used for the testing, the shortest value of t_{ph} achievable was 200 ns, increasing in steps of 32 ns, providing limited data at the turn-over of the curve shown in Figure 3(b) and therefore impacting the effectiveness of the fit to the analytical function to determine the emission time constant of the trap.

With reference to Equation 2 in which the parameter χ is included to allow for field-enhanced emission, it is possible that this spreading of the energy level of the trap could be due to field-enhanced emission or tunnelling, processes discussed in detail in [27]. Our Silvaco ATLAS semiconductor device simulations [28] of the serial register of this device indicate that an electric field of between approximately 1×10^4 and 7×10^4 Volts/cm is expected, Figure 4(a). The Poole-Frenkel effect [29] from fields of this strength would give rise to a field-induced barrier lowering (i.e. reduction in trap energy level) of between 0.02 and 0.06 eV. Energy changes of this range could be expected to give of the order of a factor of 8 variation in the emission time constant of the same trap species depending on where in the pixel the trap is located. These experimental results are consistent with such a factor and this expected variation is consistent with similar estimations in trap energy variations found in [30] in which a similar hypothesis was made. However, more specifically, the two groupings of emission times seen in Figure 6(b) may result from other possibilties, for example, different orientations of the defect in the lattice, as the silicon vacancy-oxygen defect is known to be able to exist in various orientations, as discussed by Watkins and Corbett [31] and more recently by Umeda *et al*. [32]. One alternative hypothesis to be considered is the possible presence of two defects with similar emission time constants in this temperature range, for which this separation

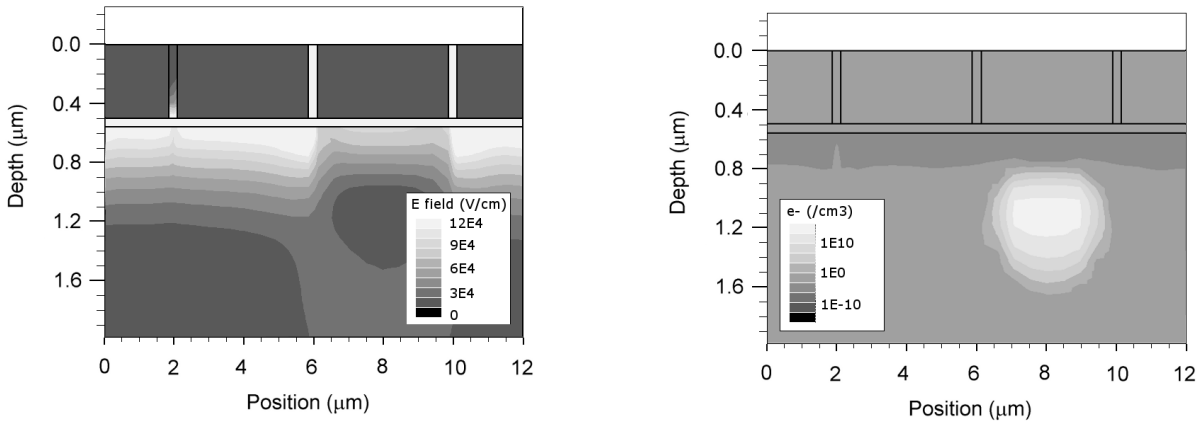

(a) Electric field strength.

(b) Electron concentration.

Fig. 4. Electric field and electron concentration for a cut through the CCD273 [26] containing approximately 26,000 electrons with a clock-high level of 7 Volts. As the electrons pass through the CCD they travel through the silicon in the region spanning a depth from 0.9 μm to 1.3 μm in (b); only traps within this region will encounter electrons and hence have the possibility to capture the electrons. The 'pumping' only occurs when traps emit electrons into a neighbouring charge packet; the same region in (a), depth from 0.9 μm to 1.3 μm, gives the electric field strength in this region and shows field strengths of approximately 1×10^4 and 7×10^4 Volts/cm (from 1.3 μm to 0.9 μm depths respectively).

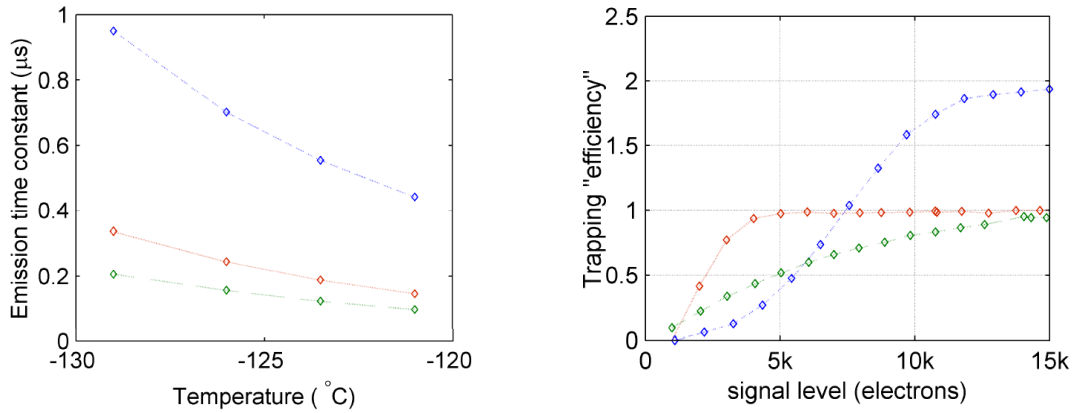

(a) The emission times are tracked across the temperature range. Error bars are approximately 4-6% (see main text).

(b) The trapping "efficiency" increases with the signal level.

Fig. 5. Examples of traps from the experimental data. The trap shown in red (solid line) is near the centre of the charge packet, rising to 100% capture probability at low signal levels whilst the trap shown in green (long dashed line) is thought to be situated towards the edge of the signal packet. The trap shown in blue (short dashed line) demonstrates that there are either two single-electron traps present under the same phase or a single two-electron trap.

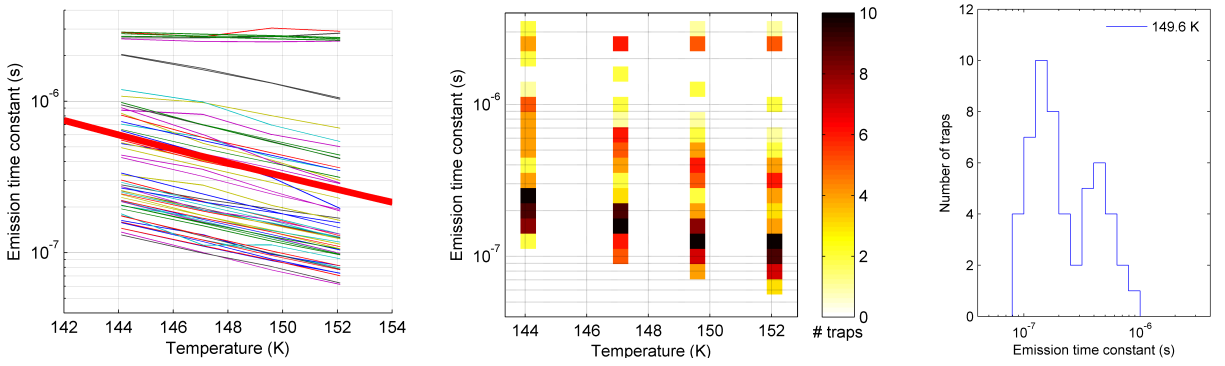

(a) Each thin line details the experimental result for a single trap.

(b) A histrogram of the data shown in (a).

(c) A single histogram from (b).

Fig. 6. Emission times constants calculated across the serial register over the four temperatures sampled. The collection of traps with negligible temperature response (longest emission times, top) are thought to due to other factors, e.g. traps under adjacent phases pumping signal against each other. The spread in the emission times is understood to be real and is explained in the text (error bars, 4-6%, for each trap are not shown to aid clarity). (a) The single thick curve shows the 'theoretical time constant' for the Si-A trap with an assumed energy of 0.17 eV and cross section of 10^{-14} cm^2 with no field enhancement [17]. (b,c) The apparent set of two main groupings emphasised more strongly in the histogram of the results will be investigated further in a future study.

would not be seen with lower resolution measurements.

VIII. Conclusions

We have combined novel analytical methods and simulations with experimental "single-trap pumping" techniques to determine the emission time constants of individual traps to an accuracy of approximately 4-6%, giving an indication that we are en route to increasing the accuracy towards the strict requirements for radiation damage correction algorithms in future missions. Here the technique has been demonstrated in a non-irradiated region of the CCD, however, the technique is equally applicable to use on irradiated devices, albeit at a low radiation dose such that the occurrence of traps remains separated by several phases in the device. By not only considering the pumping of individual traps in the temperature domain but *additionally* in the the time and signal domains, we have allowed the study of individual traps to a high level of detail, directly measuring emission time constants and capture probabilities. The technique and analysis can now be extended to include traps with the longer time constants that are more dominant during parallel transfer in the image area, such as the E-centre and divacancy. These newly-found in situ results can then be incorporated into the correction algorithms, providing a greater accuracy to the radiation damage correction process.

Acknowledgements

With thanks to Richard Massey (Durham University) for discussion of correction techniques on HST and Alex Chroneos (Open University) for interesting discussion of the Si-A. With thanks to Richard Massey and Oxford University Press for permission to reproduce Figure 1 [3].

References

[1] R. Laureijs, *et al.* (2011, Oct). Euclid Definition Study Report, ArXiv e-prints 1110.3193 [Online]. Available: http://arxiv.org/abs/1110.3193.

[2] L. Lindegren, C. Babusiaux, C. Bailer-Jones, U. Bastian, A. G. A. Brown, M. Cropper, E. Hg, C. Jordi, D. Katz, F. van Leeuwen, X. Luri, F. Mignard, J. H. J. de Bruijne and T. Prusti, "The Gaia mission: science, organization and present status", *IAU Colloq.*, vol. 248, pp. 217-223, Jul. 2008.

[3] R. Massey, "Charge transfer inefficiency in the Hubble Space Telescope since Servicing Mission 4", *MNRAS*, vol. 409, no. 1, pp. L109-L113, Nov. 2010. Fig. 3. By permission of Oxford University Press on behalf of the Royal Astronomical Society.

[4] D. Hall, J. Gow, N. Murray and A. Holland, "Optimisation of device clocking schemes to minimise the effects of radiation damage in charge coupled devices", *IEEE Trans. Electron Dev.*, vol. 59, no. 4, pp. 1099-1106, Apr. 2012.

[5] R. Massey, C. Stoughton, A. Leauthaud, J. Rhodes, A. Koekemoer, R. Ellis and E. Shaghoulian,"Pixel-based correction for charge transfer inefficiency in the Hubble Space Telescope Advanced Camera for Surveys", *MNRAS*, vol. 401, pp. 371-384, Jan. 2010.

[6] R. Massey. "Charge transfer inefficiency in the Hubble Space Telescope since Servicing Mission 4", *MNRAS*, vol. 409, no. 1, pp. L109-L113, Nov. 2010.

[7] A. Short, C. Crowley, J.H.J. de Bruijne and T. Prod'homme, "An analytical model of radiation-induced charge transfer inefficiency for CCD detectors", *MNRAS*, vol. 430, no. 4, pp. 3078-3085, Apr. 2013.

[8] M. Cropper, A. Refregier, P. Guttridge, M. Cropper, A. Refregier, P. Guttridge, O. Boulade, J. Amiaux, D. Walton, P. Thomas, K. Rees, P. Pool, J. Endicott, A. Holland, J. Gow, N. Murray, A. Amara, D. Lumb, L. Duvet, R. Cole, J.-L. Augueres and G. Hopkinson, "VIS: the visible imager for Euclid", *Proc. SPIE*, vol. 7731, pp. 77311J, Jul. 2010.

[9] J. P. D. Gow, N. Murray, A. Holland, D. Hall, M. Cropper, G. Hopkinson and L. Duvet, "Assessment of space proton radiation-induced charge transfer inefficiency in the CCD204 for the Euclid space observatory", *J. Instrum.*, vol. 7, no. 1, pp. C01030, Jan. 2012.

[10] R. Massey, H. Hoekstra, T. Kitching, J. Rhodes, M. Cropper, J. Amiaux, D. Harvey, Y. Mellier, M. Meneghetti, L. Miller, S. Paulin-Henriksson, S. Pires, R. Scaramella and T. Schrabback,"Origins of weak lensing systematics, and requirements on future instrumentation (or knowledge of instrumentation)", *MNRAS*, vol. 429, no. 1, pp. 661-678, Feb. 2013.

[11] M. Cropper, H. Hoekstra, T. Kitching, R. Massey, J. Amiaux, L. Miller, Y. Mellier, J. Rhodes, B. Rowe, S. Pires, C. Saxton and R. Scaramella, "Defining a weak lensing experiment in space", *MNRAS*, vol. 431, no. 4, pp. 3103-3126, Jun. 2013.

[12] J. Rhodes, A. Leauthaud, C. Stoughton, R. Massey, K. Dawson, W. Kolbe and N. Roe, "The effects of charge transfer inefficiency (CTI) on galaxy shape measurements", *Publ. Astron. Soc. Pac.*, vol. 122, no. 890, pp. 439-450, Apr. 2010.

[13] J. R. Srour, C. J. Marshall and P. W. Marshall, "Review of displacement damage effects in silicon devices", *IEEE Trans. Nucl. Sci.*, vol. 50, no. 3, pp. 653-670, Jun. 2003.

[14] W. Shockley and W. T. Read Jr., "Statistics of the recombinations of holes and electrons", *Phys. Rev.*, vol. 87, no. 5, pp. 835-842, Sept. 1952.

[15] R. N. Hall, "Electron-hole recombination in germanium", *Phys. Rev.*, vol. 87, no. 5, pp. 387-387, Jul. 1952.

[16] G. R. Hopkinson and A. Mohammadzadeh, "Radiation effects in charge-coupled device (CCD) imagers and CMOS active pixel sensors", *Int. J. High Speed Electr. Syst.*, vol. 14, no. 2, pp. 419-443, Jun. 2004.

[17] A. Holland, "The effect of bulk traps in proton irradiated EEV CCDs", *Nucl. Instrum. Meth. A*, vol. 326, no. 1-2, pp. 335-343, Mar. 1993.

[18] J. R. Janesick, "Charge transfer" in *Scientific charge-coupled devices*, Washington: SPIE - The International Society for Optical Engineering, 2001, ch. 5, sec. 5.3.4, pp. 430-433.

[19] N. J. Murray, A. D. Holland, J. P. D. Gow, D. J. Hall, J. H. Tutt, D. Burt and J. Endicott, "Mitigating radiation-induced charge transfer inefficiency in full-frame CCD applications by 'pumping' traps", *Proc. SPIE*, vol. 8453, pp. 845317, Jul. 2012.

[20] D. V. Lang, "Deep-level transient spectroscopy: A new method to characterize traps in semiconductors", *J. Appl. Phys.*, vol. 45, no. 7, pp. 3023-3032, Jul. 1974.

[21] C. Bebek, D. E. Groom, S. E. Holland, A. Karcher, W. F. Kolbe, J. S. Lee, M. E. Levi, N. P. Palaio, B. T. Turko, M. C. Uslenghi, M. T. Wagner, and G. Wang, "Proton radiation damage in high-resistivity n-type silicon CCDs", *Proc. SPIE*, vol. 4669, pp. 161-171, Apr. 2002.

[22] N. J. Mostek, C. J. Bebek, A. Karcher, W. F. Kolbe, N. A. Roe and J. Thacker, "Charge trap identification for proton-irradiated p+ channel CCDs", *Proc. SPIE*, vol. 7742, pp. 774216, Jul. 2010.

[23] D. Hall, A. Holland, N. Murray, J. Gow and A. Clarke, "Modelling charge transfer in a radiation damaged charge coupled device for Euclid", *Proc. SPIE*, vol. 8453, pp. 845315, Jul. 2012.

[24] A. Clarke, D. Hall, A. Holland and D. Burt, "Modelling charge storage in Euclid CCD structures", *J. Instrum.* vol.7, no. 1, pp. C01058, Jan. 2012.

[25] A. Clarke, D. Hall, N. Murray, A. Holland and D. Burt, "Device modelling and model verification for the Euclid CCD273 detector", *Proc. SPIE*, vol. 8453, pp. 84531I, Jul. 2012.

[26] J. Endicott, S. Darby, S. Bowring, T. Eaton, A. Grey, I. Swindells, R. Wheeler, L. Duvet, M. Cropper, D. Walton, A. Holland, N. Murray and J. Gow, "Charge-coupled devices for the ESA Euclid M-class mission", *Proc. SPIE*, vol. 8453, pp. 845301, Jul. 2012.

[27] P. A. Martin, B. G. Streetman and K. Hess, "Electric field enhanced emission from non-Coulombic traps in semiconductors", *J. Appl. Phys.*, vol. 52, no. 12, pp. 7409-7415, Dec. 1981.

[28] Manual, *ATLAS Users*, Santa Clara: Silvaco International, 2000.

[29] J. Frenkel, "On pre-breakdown phenomena in insulators and electronic semi-conductors", *Phys. Rev.*, vol. 54, no. 8, pp. 647-648, Oct.1938.

[30] K. D. Stefanov, T. Tsukamoto, A. Miyamoto, Y. Sugimoto, N. Tamura, K. Abe, T. Nagaminc and T. Aso, "Electron and neutron radiation damage effects on a two-phase CCD", *IEEE Trans. Nucl. Sci.*, vol. 47, no. 3, pp. 1280-1291, Jun. 2000.

[31] G. D. Watkins and J. W. Corbett, "Defects in irradiated silicon. I. Electron spin resonance of the Si-A center", *Phys. Rev.*, vol. 121, no. 4, pp. 1001-1014, Feb. 1961.

[32] T. Umeda, K. Okonogi, K. Ohyu, S. Tsukada, K. Hamada, S. Fujieda and Y. Mochizuki, "Single silicon vacancy-oxygen complex defect and variable retention time phenomenon in dynamic random access memories", *Appl. Phys. Lett.*, vol. 88, pp. 253504, Jun. 2006.